This paper is submitted to the Special Issue of JAM corresponding to the ENIEF'2004 Conference

Guest Editors Buscaglia & Younis

Numerical Simulation of Transient Free Surface Flows Using a Moving Mesh Technique

Laura Battaglia, Jorge D'Elía, Mario Storti, and Norberto Nigro

Centro Internacional de Métodos Computacionales en Ingeniería (CIMEC)
Instituto de Desarrollo Tecnológico para la Industria Química (INTEC)
Universidad Nacional del Litoral - CONICET
Güemes 3450, 3000-Santa Fe, Argentina
Tel.: (+54) 0342-4511594/5 - Fax: (+54) 0342-4511169
e-mail: lbattaglia@ceride.gov.ar,
(jdelia, mstorti, nnigro)@intec.unl.edu.ar
web page: http://venus.ceride.gov.ar/CIMEC

Abstract

In this work, transient free surface flows of a viscous incompressible fluid are numerically solved through parallel computation. Transient free surface flows are boundary-value problems of the moving type that involve geometrical nonlinearities. In contrast to more conventional computational fluid dynamics (CFD) problems, the computational flow domain is partially bounded by a free surface which is not known a priori, since its shape must be computed as part of the solution. In steady-flow the free surface is obtained by an iterative process, but when the free surface evolves with time the problem is more difficult as it generates large distortions in the computational flow domain. The incompressible Navier-Stokes numerical solver is based on the finite element method with equal order elements for pressure and

velocity (linear elements), and it uses a Streamline Upwind/Petrov-Galerkin (SUPG) scheme (Hughes, T. J. R. and Brooks, A. N., 1979, "A Multidimensional Upwind Scheme With no Crosswind Diffusion", In Finite Element Methods for Convection Dominated Flows, ASME ed., **34.**AMD, New York, pp. 19-35, and Brooks, A. N., and Hughes, T. J. R., 1982, "Streamline Upwind/Petrov-Galerkin for Convection Dominated Flows With Particular Emphasis on the Incompressible Navier-Stokes Equations", Comput. Methods Appl. Mech. Eng.,**32**, pp. 199-259) combined with a Pressure-Stabilizing/Petrov-Galerkin (PSPG) one (Tezduyar, T. E., 1992, "Stabilized Finite Element Formulations for Incompressible Flow Computations", Adv. Appl. Mech., **28**, pp. 1-44, and Tezduyar, T. E., Mittal, S., Ray, S. E., and Shih, R., 1992, "Incompressible Flow Computations With Stabilized Bilinear and Linear Equal Order Interpolation Velocity-Pressure Elements", Comp. Methods Appl. Mech. Eng., **95**, pp. 221-242). At each time step, the fluid equations are solved with constant pressure and null viscous traction conditions at the free surface and the velocities obtained in this way are used for updating the positions of the surface nodes. Then, a pseudo elastic problem is solved in the fluid domain in order to relocate the interior nodes so as to keep mesh distortion controlled. This has been implemented in the PETSc-FEM code (PETSc-FEM: a General Purpose, Parallel, Multi-Pysics FEM Program. GNU General Public License (GPL), http://www.cimec.org.ar/petscfem) by running two parallel instances of the code and exchanging information between them. Some numerical examples are presented.

1 Introduction

Free surface flows are very common in engineering problems. They include for instance the sloshing case which appears in vehicle, ship or aerospace engineering, when the back-and-forth splashing of a liquid fuel in its tank can lead to problems of stability and control in ground or launch vehicles. Another case is the sloshing in a liquid storage tank subjected to seismic action when high impact loads on the tank roof and walls can damage the liquid storage tank. Early simulations of the liquid sloshing problem in a liquid carrier or storage tanks have mostly been performed with waves of small steepness assuming low sloshing so that the nonlinear boundary conditions can be neglected.

The most commonly applied classic idealization for estimating liquid response in excited rigid tanks is Housner's [1]. The hydrodynamic pressures are divided into two components: the impulsive pressure caused by the portion of liquid accelerating with the tank, and the convective pressure caused by the portion of liquid sloshing in the tank. These hydrodynamic pressures result in added masses which can duplicate forces and moments exerted by a liquid on a vibrating tank, as shown in the computations reported in Ref. [2]. Sloshing in a more general context is extensively reviewed by Biswal *et al.* [3].

From a numerical point of view, several techniques have been developed for the solution of free surface flows as initial value problems. These techniques are roughly classified by Shyy *et al.* [4] as Eulerian, Lagrangian, or mixed Eulerian-Lagrangian.

In Eulerian-like (volume-tracking) approaches (see Fig. 1), the mesh remains stationary or moves in a predetermined manner. Moreover, the free surface is not explicitly tracked but it is reconstructed from other field properties such as the fluid fractions. Then, the fluid moves in/out of the computational flow domain. Under this scope, Aliabadi and Tezduyar [5] performs a numerical simulation of sloshing in tanker trucks during turning with a stabilized finite element formulation which is implemented in parallel using the message-passing interface libraries. The level set method, the well known "Marker-And-Cell" (MAC) method, and immersed boundary methods are schemes of this type (e.g. see Perot and Nallapati [6]). They can handle large displacements without loss of accuracy. impose the free boundary conditions, due to a lack of a sharp definition, see Nickell *et al.* [7], Silliman and Scriven[8], Ruschak[9] and Kawahara and Miwa[10]. In Lagrangian-like (surface-tracking) approaches, the mesh is configured to conform to the shape of the free surface, i.e., it continually adapts to it. The free surface is a discontinuity whose evolution is explicitly tracked as an $(n-1)$ dimensional entity in an n-dimensional space. No modeling is necessary to define the free surface or its effects on the flow field because the grid points move with the local fluid particles. However, mesh movement or remeshing is usually necessary for large deformations, see Bach and Hassager[11] and Ramaswamy and Kawahara[12]. In mixed Eulerian Lagrangian-like approaches, or Arbitrary Lagrangian-Eulerian (ALE) formulations, the advantages of both methods are taken into account, see Hughes *et al.*

[13], or more recently Sung *et al.* [14]. Other mixed approaches are also proposed. For example, the "emplicit" method uses an explicit-implicit time integration oriented to seakeeping ship motions, see Huang and Sclavounos[15], while the "material point" method, see York *et al* [16], uses unconnected Lagrangian points and a background Eulerian mesh for solving fluid-membrane interaction.

While kinematic and dynamic laws govern the displacement of the computational flow domain at the moving boundaries, in Lagrangian-like (surface-tracking) approaches the motion of the internal nodes is largely arbitrary. A primary criterion is to achieve absorption of expected boundary displacements while keeping or controlling the distortion of the mesh elements, which are assumed to be well-shaped at the start of the simulation. A number of possibilities have been proposed; they can be roughly classified in three main strategies (e.g. see Tezduyar *et al.*) [17]:

1. *algebraic mesh update*: it applies an explicit algebraic expression for the displacement of each interior node as a function of the displacement of one or more boundary nodes;

2. *pseudo-elastic mesh update* [18, 19]: it embeds the mesh in an elastic pseudo-solid governed by a fictitious constitutive relation and solves a boundary value problem with imposed boundary displacements. The mesh updates based on using different ratios of the Lamé constants were introduced by Johnson and Tezduyar[19], and results were reported as a function of that ratio;

3. *mesh update through regeneration*: it performs an entirely new mesh based on the updated boundary locations and projects the solution from the old mesh to the new one.

In a previous study[20], a Lagrangian-type panel method in the time domain was proposed for inviscid potential flows with a moving free surface where the instantaneous velocity-potential and normal displacement on the moving free surface were obtained by means of a time-marching scheme after a spatial semi-discretization with a low-order scheme. Later[21], a surface reallocation strategy for the instantaneous wet hull surface caused by changes in the position of the intersection curve between the free surface and hull surface was shown.

In this work, a mesh-movement technique for transient flow domains with a free surface of a viscous and incompressible fluid is addressed in the context of a finite element approach and solved by parallel computation.

2 Governing equations

The flow of an incompressible and viscous fluid of the Newtonian type is considered. The governing flow equations are the Navier-Stokes (NS) ones,

$$\begin{aligned} \rho\left(\partial_t \boldsymbol{v} + \boldsymbol{v}\cdot\nabla\boldsymbol{v} - \boldsymbol{f}\right) - \nabla\cdot\boldsymbol{\sigma} = 0 \ ; \\ \nabla\cdot\boldsymbol{v} = 0 \ ; \end{aligned} \tag{1}$$

on the flow domain $\Omega_t = \Omega(t)$ at time t, for all $t \in [0, T]$, where $\boldsymbol{v}$ is the fluid velocity, $\boldsymbol{f}$ is the body force, ρ is the fluid density and T is a final time. The fluid stress tensor $\boldsymbol{\sigma}$ is decomposed into its isotropic $-p\boldsymbol{I}$ and deviatoric $\boldsymbol{T}$ parts

$$\boldsymbol{\sigma} = -p\boldsymbol{I} + \boldsymbol{T} \ ; \tag{2}$$

where p is the pressure and $\boldsymbol{I}$ is the identity tensor. As only Newtonian fluids with constant physical properties are considered, its deviatoric part $\boldsymbol{T}$ is related linearly to the strain rate tensor with

$$\boldsymbol{T} = 2\mu\boldsymbol{\epsilon} \quad ; \quad \boldsymbol{\epsilon} = \frac{1}{2}\left[\nabla\boldsymbol{v} + (\nabla\boldsymbol{v})^T\right] \ ; \tag{3}$$

where μ and $\nu = \mu/\rho$ are the dynamic and kinematic viscosity of the fluid and $(...)^T$ denotes the transpose. The boundary conditions are

$$\begin{aligned} \boldsymbol{v} &= 0 \qquad \text{at } \Gamma_{wall}; \\ p &= P_{\text{atm}} \quad \text{at } \Gamma_{FS}; \\ \boldsymbol{\tau}\cdot\boldsymbol{n} &= 0 \qquad \text{at } \Gamma_{FS}; \end{aligned} \tag{4}$$

where Γ_{wall} is the boundary on the solid walls while Γ_{FS} is the free surface. Note that as no restriction is imposed on velocity at the free surface, then the normal velocity there can be non-null. This normal velocity

is responsible of the free surface movement. The boundary conditions at the free surface are similar to those normally imposed at an outlet boundary. ALE terms [13] are included in order to take into account the advection of momentum caused by the relocation of the nodes.

The discretization of this system of Partial Differential Equations (PDE) is carried out by a finite element method based on the Streamline Upwind/Petrov-Galerkin (SUPG) [22, 23] and Pressure-Stabilizing/Petrov-Galerkin (PSPG) [24, 25] formulations. This leads to a set of Ordinary Differential Equation (ODE) in time, which is discretized by a finite difference method. A trapezoidal integration rule is employed for solving this ODE, which has been verified to be second order for $\alpha = 0.5$ in the numerical examples (it is often used $\alpha = 0.6$).

At each time step, a non-linear system of equations of the form

$$\boldsymbol{F}\left(\frac{\boldsymbol{v}^{n+1}-\boldsymbol{v}^{n}}{\Delta t}, \boldsymbol{p}^{n+1}\right) = \mathbf{o} \ ; \tag{5}$$

is obtained so that having setting the state of the fluid at time t^n and a mesh for the domain $\Omega(t^n)$, the velocity and pressure unknowns at time t^{n+1} can be solved. As the velocity may be non-null at the free surface in a Lagrangian approach, the nodes there should move with velocity

$$\boldsymbol{v}_j^{n+1} \approx \frac{\boldsymbol{x}_j^{n+1}-\boldsymbol{x}_j^{n}}{\Delta t} \ . \tag{6}$$

However, displacements of the nodes tangential to the free surface are considered irrelevant so that it is necessary to verify only the normal component of this equation

$$\left(\frac{\boldsymbol{x}_j^{n+1}-\boldsymbol{x}_j^{n}}{\Delta t} - \boldsymbol{v}_j^{n+1}\right) \cdot \ \boldsymbol{n}_j^n = 0 \ . \tag{7}$$

In addition, the movement of the free surface nodes are constrained along a fixed direction $\hat{\boldsymbol{s}}_j$, then

$$\boldsymbol{x}_j(t) = \boldsymbol{x}_{0,j} + \eta_j(t) \ \hat{\boldsymbol{s}}_j \ ; \tag{8}$$

where η_j is a scalar coordinate along some *"spine"* whose direction is $\hat{\boldsymbol{s}}_j$ and starting point $\boldsymbol{x}_{0,j}$, see Fig. 2. Then Eq. (5) gives an equation for the increment in η coordinate

$$\Delta\eta_j^{n+1} = \eta_j^{n+1} - \eta_j^n = \Delta t \frac{\boldsymbol{v}_j^{n+1} \cdot \hat{\boldsymbol{n}}_j^n}{\hat{\boldsymbol{s}}_j \cdot \hat{\boldsymbol{n}}_j^n} \ . \tag{9}$$

Note that the spines $(\boldsymbol{x}_{0,j}, \hat{\boldsymbol{s}}_j)$ do not change with time. The only requirement is that the spine direction and the normal be non-orthogonal at each node at each time step, which means that the fixed direction can be defined almost arbitrary. However, it is convenient to choose them as parallel as possible to the expected surface normal. For example, the spines for a spillway are usually drawn perpendicular to the main profile of the structure. These spines are only used for the movement of the free surface nodes, that is, the interior ones are relocated by solving the pseudo elastic problem regardless of spines directions. On the other hand, the normal to the free surface at node $\boldsymbol{x}_j$ is computed at each time step using

$$\begin{aligned} \hat{\boldsymbol{n}} &\propto \int_{FS} N_j(\boldsymbol{x}) \hat{\boldsymbol{n}}(\boldsymbol{x}) d\boldsymbol{\Sigma}_{FS} \ ; \\ \|\hat{\boldsymbol{n}}_j\| &= 1 \ ; \end{aligned} \tag{10}$$

where $N_j(\boldsymbol{x})$ is the finite element interpolation for the j-node and $\hat{\boldsymbol{n}}(\boldsymbol{x})$ is the normal to the free surface at point $\boldsymbol{x}$. The integration is carried out over the whole free surface, but due to the local support of the finite element interpolation function it involves only those elements that are connected to the j-node. For linear tetrahedral elements in the fluid, this amounts to the weighted average of the normals of the triangular panels around the j-node.

Other limitations of the method of spines are inclined walls or high velocity normal to the spines, all situations that could also appear simultaneously. Considering that displacements are projected onto the direction of the spines, all these cases produce loss of information or instabilities over the free surface. An alternative to reduce negative aspects of spines direction is proposed by Behr and Abraham[26], who treated in the referenced paper an application for inclined walls problems. It must be emphasized that unlike this method, which uses the projection over fixed spines only for the free-surface, other proposals project the displacements of all the nodes over fixed directions. As a consequence of this, the mesh updated by the elastic solver is less distorted than in other proposals.

3 Moving mesh strategy

Once the displacements of the free surface nodes at time step $n+1$ are known, the positions of the internal nodes can be moved so as to reduce the distortion of the mesh elements. Here, an implementation of the *pseudo-elastic mesh update* strategy is employed. It is based on solving an artificial elastic problem with imposed displacements at the free surface, and slip or non-slip conditions at solid walls and other boundaries, see Tezduyar *et al.* [18] or Johnson[19]. Consider for instance a typical case of a truck container as in Fig. 10 with a separating wall. Under longitudinal accelerations of the truck, the fluid tends to go from one half to the other causing large displacements of the fluid surface with extreme positions as shown in Fig. 3. Under these circumstances, the best boundary conditions for the pseudo elastic problem may be to let the nodes move freely at the solid walls $ABCD$, GH and IE (slip boundary condition). However, these can cause large distortions of the elements near the tip F of the separator, so a non-slip one is imposed in a small region around the tip, such as the portion HFI.

The pseudo elastic problem may be posed as

$$\begin{aligned} \sigma_{ij,j} &= 0 \ ; \\ \sigma_{ij} &= 2\tilde{\mu}\epsilon_{ij} + \tilde{\lambda}\delta_{ij}\epsilon_{kk} \ ; \\ \epsilon_{ij} &= \frac{1}{2}(u_{i,j} + u_{j,i}) \ ; \end{aligned} \tag{11}$$

where $\boldsymbol{u}$ is the mesh node displacements

$$\boldsymbol{u}_j = \boldsymbol{x}_j^{n+1} - \boldsymbol{x}_j^0 \ ; \tag{12}$$

where $\tilde{\mu}$ and $\tilde{\lambda}$ are the Lamé elastic constants for the fictitious elastic material and δ_{ij} is the Kronecker tensor. Of course, the pseudo elastic problem is invariant under a multiplicative constant in the elastic coefficients since only Dirichlet conditions are used. The only relevant parameter is the ratio between them, or its equivalent, the Poisson ratio $\tilde{\nu}$. The Lamé constants $\tilde{\mu}$ and $\tilde{\lambda}$ can be expressed in terms of more

familiar modulus of elasticity $\tilde{E}$ with

$$\tilde{\mu} = \frac{\tilde{E}}{2(1+\tilde{\nu})} \quad ; \quad \tilde{\lambda} = \frac{\tilde{\nu}\tilde{E}}{(1+\tilde{\nu})(1-2\tilde{\nu})} \ . \tag{13}$$

It is not clear which values are more appropriate for $\tilde{\nu}$ but for $\tilde{\nu} \to 1/2$ the material is nearly incompressible and the pseudo elastic problem will become ill conditioned. The increment of the Poisson ratio towards the incompressible limit ($\tilde{\nu} = 0.5$) tends to increase the ability to admit larger displacements of the free surface without collapse but for small deformations of the free surface, lower values of $\tilde{\nu}$ can be used. In [19], this moving mesh method was reported, including several examples and the study of the influence of the Lamé constants was considered. The interest in using lower values of $\tilde{\nu}$ is achieving a better conditioning of the pseudo-elastic problem, and then a lower computational cost. In the numerical examples, $\tilde{\nu} = 0.3$ was used for moderate free surface deformations and $\tilde{\nu} = 0.45$ for larger ones.

The boundary conditions are

$$\boldsymbol{u} = \Delta\boldsymbol{x}^{n+1} \text{ at free surface } AG + ED; \tag{14}$$

$$\boldsymbol{u} = 0 \qquad \text{at non-slip boundary } HFI; \tag{15}$$

$$\boldsymbol{u} \cdot \hat{\boldsymbol{n}} = 0 \qquad \text{at slip boundary } ABCD + GH + IE; \tag{16}$$

where $\Delta\boldsymbol{x}^{n+1} = \boldsymbol{x}^{n+1} - \boldsymbol{x}^0$. The pseudo elastic problem is solved in the reference mesh Ω_0, where the choice between slip and non-slip boundary condition at solid walls is problem dependent and is specified by the user. Once this problem is solved, the updated position of the internal nodes $\boldsymbol{x}^{n+1}$ is obtained with Eq. (12).

Several alternatives for the mesh relocation problem could be devised. Non-linear elastic material behavior could be used in order to reduce distortion but in the linear version shown here the computing time per time step and memory requirements are lower than the ones needed for the fluid, and it was able to solve problems with relatively large distortions, as shown in the examples below.

4 Free surface elevation smoothing

The whole algorithm as described so far is unstable for gravity waves of high frequency and must be stabilized, mainly due to the fully explicit character of the free surface update given by Eq. (9). This has been also reported by other authors[27]. In this study, a smoothing operator is applied to the free surface elevation so that Eq. (9) is replaced by

$$\begin{aligned} \Delta\tilde{\eta}_j^{n+1} &= \frac{\boldsymbol{v}_j^{n+1} \cdot \hat{\boldsymbol{n}}_j^n}{\hat{\boldsymbol{s}}_j \cdot \hat{\boldsymbol{n}}_j^n} \ ; \\ \Delta\eta_j^{n+1} &= \mathcal{S}(\Delta\tilde{\eta}_j^{n+1}) \ ; \end{aligned} \tag{17}$$

where $\mathcal{S}$ is a smoothing operator based on solving the heat equation with a diffusivity α adjusted so as to have a characteristic spreading length γh, where h is a characteristic global mesh size, and γ is a user chosen parameter; usually, $\gamma = 2$ is employed.

5 Moving contact line

As described so far, the nodes at the contact line (i.e. the intersection of the free surface with a wall boundary, also called waterline) have null velocity due to how boundary conditions are imposed, leading to large elevation gradients near the wall. The non-slip condition may be relaxed at the contact line and replaced by the Navier slip condition

$$(\boldsymbol{I} - \boldsymbol{nn}) \cdot (\boldsymbol{n} \cdot \boldsymbol{\sigma}) = -\frac{1}{\beta}(\boldsymbol{I} - \boldsymbol{nn}) \cdot (\boldsymbol{v} - \boldsymbol{v}_{\text{wall}}) \ ; \tag{18}$$

where $\boldsymbol{v}$ is the fluid velocity at the contact line, $\boldsymbol{v}_{\text{wall}}$ is the wall velocity, $\boldsymbol{I} - \boldsymbol{nn}$ is the projector onto the tangent plane and β is an empirical slip coefficient. For $\beta = 0$ the non-slip condition is considered, whereas for $\beta \to \infty$ the perfect slip condition is recovered.

In the cases evaluated up to now, the contact line movement is implemented over a thin strip of nodes near the free surface or only those nodes which define the contact line, over the walls, whose nodal displacements are controlled by this condition.

6 Numerical results

6.1 Some comments on the viscous incompressible Navier-Stokes solver

This section depicts the ability of the incompressible Navier-Stokes module implemented in the PETSc-FEM library [28] to capture the physics involved in the flow of a viscous incompressible fluid, i.e., vorticity, transport and dissipation. Both, the Navier-Stokes solver and the linear system solver, based on domain decomposition techniques, were applied to different benchmarks in order to prove its validity, accuracy and efficiency [29, 30, 31].

In particular, the laminar flow past a circular cylinder at moderated Reynolds numbers is proposed. Much research work focused on the description of this problem, from the experimental and numerical point of view, covering a wide range of Reynolds numbers, see Refs. [32, 33, 34, 35, 36, 37, 38, 39, 40]). This fact had pushed to CFD community to use this test as a benchmark to validate CFD code development. Results obtained from PETSc-FEM show good agreement with those published in the references above. A maximum error of 0.5% in the prediction of the Strouhal number is verified, while a maximum error of 2.5% in the predicted lift and drag forces is encountered.

6.2 Analytic validation: 2D viscous sloshing

For validating the proposed method, a twodimensional (2D) sloshing test with analytical solution is performed, following Rabier and Medale[41]. This test mainly shows how a numerical scheme predicts, besides the frequency, the damping rate governed by the fluid viscosity. It consists in solving the initial-value problem of the small-amplitude motion of the free surface of a viscous fluid in a rectangular tank, see Fig. 4, whose free surface is in an initial position given by

$$h(x) = 1.5 + a_0 \sin[\pi(1/2 - x)] \; ; \tag{19}$$

where a_0 is the amplitude of the initial sinusoidal perturbation of the movement. The fluid is submitted to gravity acceleration, and viscous forces are responsible for the damping of movement. The boundary

conditions chosen are perfect slip on solid boundaries, as mentioned in section §5, i.e., null normal velocity and tangential stresses, and over the free surface, $p = P_{\text{atm}}$ and $\boldsymbol{\tau} \cdot \boldsymbol{n} = 0$. The analytical solution of the linearized case is given by Prosperetti[42] as

$$a(t) = \frac{4\nu^2 k^4}{8\nu^2 k^4 + {\omega_0}^2}\, a_0\, \text{erfc}(\nu k^2 t)^{1/2} + \sum_{i=1}^{4} \frac{z_i}{Z_i} \left(\frac{\omega_0^2 a_0}{z_i^2 - \nu k^2} \right) \exp[(z_i^2 - \nu k^2)t]\, \text{erfc}(z_i t^{1/2}) \; ; \tag{20}$$

where ν is the kinematic viscosity of the fluid, k is the wave number, $\omega_0^2 = gk$ is the inviscid natural frequency, each z_i is the root of the following algebraic equation

$$z^4 + k^2 \nu z^2 + 4(k^2\nu)^{3/2} z + \nu^2 k^4 + \omega_0^2 = 0 \; ; \tag{21}$$

where $Z_1 = (z_2 - z_1)(z_3 - z_1)(z_4 - z_1)$ with Z_2, Z_3, Z_4 obtained by circular permutation of the indices and erfc(...) is the error function for complex variable. This expression is valid for small-amplitude flat waves in an infinite depth domain.

The example was solved for the chosen geometry, with initial maximum perturbation $a_0 = 0.01$ m, kinematic viscosity $\nu = 0.01$ m^2/s, unit gravity acceleration $g = 1.0$ m/s^2 and a mesh of 40×60 quadrangular elements for the container of $h = 1.5$ m height and $d = 1.0$ m wide, with a time-step $\Delta t = 2.12\ 10^{-2}$ s.

In Fig. 5, the vertical position of the upper left node versus time is plotted over the curve calculated analytically.

The results obtained allow validation of the method, considering the capture of the frequency and the rate of viscous damping in the experiment.

6.3 Analytic validation: 3D quasi-inviscid sloshing

The proposed case corresponds to a right cylinder of annular base, as shown in Fig. 6. The nature of this problem is clearly 3D because of the initial condition imposed, which produces fluid circulation from one side to the other of the tank. This test mainly shows how the numerical scheme simulates the eigenvalues and eigenmodes of the free surface, e.g. see Papaspyrou[43] *et al.*.

The internal radius of the cylinder is $R_i = 1.0$ m, and the external one $R_e = 2.0$ m. The initial condition proposed, represented also in Fig. 6, is the free surface perturbed by displacements given by the natural frequency $n = 1$, with maximum amplitude $a_0 = 0.05$ m over fluid height, $h = 1.0$ m. In this way, the movement is not influenced by natural modes other than the one used as initial condition.

As in the precedent case, boundary conditions are imposed as follows: $p = P_{\text{atm}}$ and $\boldsymbol{\tau} \cdot \boldsymbol{n} = 0$ over the free surface, and perfect slip on solid walls.

The results obtained are contrasted with equations developed by Moiseev and Petrov [44], which calculate natural frequencies of sloshing for inviscid liquids in this kind of domains. As this analytical value is computed under the inviscid hypothesis, it is not expected that the numerical viscous value converge to it, even when $\nu \to 0$ and the mesh is refined. However it is expected to give a good approximation with a small percentage of relative error.

For the natural frequency ω, the wave number k and the dimensionless coefficient $c = R_e/R_i > 1$, the equations considered are

$$k_m^{(n)} = \frac{\left(\omega_m^{(n)}\right)^2}{g}; \tag{22}$$

$$k_m^{(n)} = \kappa_m^{(n)} \tanh[\kappa_m^{(n)}\ h]; \tag{23}$$

where $\kappa_m^{(n)}$ is the mth root of the equation

$$J_n'(\kappa) \cdot N_n'(c\kappa) - N_n'(\kappa) \cdot J_n'(c\kappa) = 0; \tag{24}$$

in which $J_n(...)$ and $N_n(...)$ are Bessel functions of first and second kind, respectively. Besides, $n = 1$ was adopted corresponding to the lowest frequency mode. The higher periods calculated by applying this method are $T_1 = 9.94$ s, $T_2 = 3.47$ s, $T_3 = 2.49$ s and $T_4 = 2.04$ s, considering that $T = 2\pi/\omega$. As the first is the leading one, $T_a = 9.94$ s is used as analytical period for comparing to numerical results.

The finite element problem for this case was solved with a mesh of 32000 hexahedral 8-node elements and 35721 nodes, with gravity $g = 1.0$ m/s^2, kinematic viscosity $\nu = 10^{-3}$ m^2/s and $\Delta t = 0.1$ s.

Numerical results are plotted in Fig. 7, where vertical displacements of four representative nodes are plotted making it possible to distinguish the period T of the movement. A global way to show the sloshing is proposed, in this case the free surface nodal displacements weighted with a "first moment function" (see Fig. 8). This function calculates the sum of nodal vertical displacements multiplied by its distance to the axis of the cylinder, allowing the estimation of the experimental period for the whole tank, as the average of time differences between the zeros of the function. The period of movement calculated in this way is $T_e = 10.33$ s. The relative error between the numerical viscous solution and the inviscid one is under 4%.

Several analysis were made for studying convergence of the method, taking the period of the movement as the main parameter. The variables considered were the mesh mean step h and the time step, keeping the quotient between them constant. Considering that the finite element approximation applied is $O(h^2)$, the results were used to make a Richardson's extrapolation which gave an asymptotic $T_0 = 10.315$ s for $h \to 0$. In Fig. 9, the calculated points are plotted, as well as T_0.

6.4 Example: tank with internal buffer

A truck-like container tank with an internal buffer subject to an impulsive deceleration is considered (see Fig. 10). The container is moving right at velocity 0.5 m/s and suddenly stops at $t = 0$ s. The tank length and width are $L = 1.20$ m and $L_y = L/2$ m, respectively, and the curvature radius of tank corners is $R_C = 0.15$ m. The length of wall edge separation is $W = 0.15$ m. The starting height of fluid in the tank is $H_f = 0.36$ m. In this example, the perfect slip condition (see section §5) is used on the contact line and the nodes on a thin strip near the contact line, whose width is $H_s = 0.2 \times H_f = 0.072$ m. The number of elements in fluid movement direction is 80, the same as in the wall-to-wall directions and in the crossing one (see Fig. 11). The time step is $\Delta t = 0.02$ s, the gravity acceleration $g = 9.81$ m/s^2 and the kinematic viscosity is $\nu = 3 \times 10^{-5}$ m^2/s.

The internal buffer is a wall edge separation that is placed to break the fundamental longitudinal sloshing mode. Nevertheless, with this geometrical container configuration and under longitudinal accelerations or

decelerations, there is a transient back-and-forth splashing of the liquid, as a hydraulic pendulum. The observed period of the main mode is $T_h \approx 1.7$ s. As the fluid passes from the right half to the left one there is a strong viscous friction near the tip of the separator. This causes emission of vortices, which are the main energy dissipation mechanism. Figures 12 and 13 correspond to time instants near the point of maximum height in the left half. A forming vortex is clearly seen in Fig. 12 on the left wall of the separator near the tip. In Fig. 13 it has already been separated from the wall. Once the vortices are shed, they are transported by the fluid and in Figs. 14 and 15 the vortex is passing to the right half and a new vortex is forming on the right half.

The Reynolds number (Re) observed in the region where the vortices are shed is low enough (Re ≈ 100) to make a turbulence model unnecessary, so the vorticity is a result of the averaged Navier-Stokes equations, which are accurately solved by the corresponding PETSc-FEM module, as mentioned in section §6.1.

7 Conclusions

In this study a moving mesh technique for transient free surface flows of an incompressible and viscous fluid of Newtonian type, in the context of SUPG and PSPG formulations for finite elements is shown.

The combined fluid and moving mesh problem was formulated within the picture of the multi-physics programming paradigm, and was implemented reusing preexistent fluid and elastic modules which are not specifically oriented to the free surface case.

Numerical tests show that the frequency and damping of sloshing modes are accurately predicted. Even if the surface elevation is updated with an explicit strategy, time steps as large as one twentieth of the main sloshing mode period can be used. The simple moving mesh strategy based on a linear pseudo-elastic operator proved to be robust enough, allowing large surface elevation amplitudes.

The right cylinder of annular base example shows that the method can be applied in 3D and more complex geometries with structured or unstructured meshes composed of any combination of tetrahedral,

hexahedral and wedge elements.

The advantages of this technique over those with remeshing are related to the computational cost of the pseudo elastic problem, which is smaller than a whole remeshing, and the possibility of parallelizing the pseudo-elastic problem.

Future work will involve the inclusion of more complex moving mesh strategies involving non-linear pseudo-elastic models. In sloshing applications, modeling will be focused on how to couple the dynamics of the fluid with the container dynamics, for instance, the simulation of sloshing in containers on tanker trucks with accelerations during turning.

Acknowledgments

This work was partially performed with the *Free Software Foundation/GNU-Project* resources as `GNU/Linux OS` and `GNU/Octave`, as well another Open Source resources as `PETSc`, `MPICH` and `OpenDX`, and supported through grants CONICET-PIP-02552/2000, ANPCyT-FONCyT-PME-209 **Cluster**, ANPCyT-FONCyT-PID-99-74 **Flags**, ANPCyT-PICT-6973-BID-1201/OC-AR **Proa** and CAI+D-UNL-2000-43.

A Appendix: Parallel and multi-physics implementation details

Besides being relevant from the physical and engineering point of view, this problem is interesting as a paradigm of multi-physics programming. Even if it is perfectly possible to implement it as a module, it is interesting to see how it is implemented reusing preexistent fluid and elastic modules which are not specifically oriented to the free surface case. The proposed algorithm is implemented in the PETSc-FEM[29, 28] code, which is a parallel multi-physics finite element program based on the Message Passing Interface MPI[45] and the Portable Extensible Toolkit for Scientific Computations PETSc[46]. Among CFD applications, this flow-solver includes, for instance, hydrology [30] and free surface flows [20, 47].

The pseudo-elastic and fluid problems are run in independent PETSc-FEM instances, both in parallel. In general, there is a PETSc-FEM process for the flow problem and another for the pseudo-elastic one

at each computing node. The key point in the implementation is the data exchange and synchronization between both parallel processes. This could be done by modifying the PETSc-FEM sources or by writing a small script or C++ external code that communicates with both PETSc-FEM processes. Instead of this alternatives, PETSc-FEM has a feature called *"hooks"* that are C++ modules, or eventually shell scripts (bash, Perl, Python or other), that are run at certain specific points in the program. This concept was borrowed from the `GNU Emacs` editor and also from the Linux [48] kernel. The C++ hooks are compiled and dynamically loaded at runtime, so that it is not necessary to link them against PETSc-FEM or modify the sources. Currently, the Navier-Stokes PETSc-FEM module launches hooks at 4 points in the execution thread: before the beginning of the time step loop, at the beginning and end of each time step, and after the time step loop.

For the problem at hand two PETSc-FEM C++ hooks were written, one that is executed from the NS process and the other from the pseudo-elastic mesh-relocation process. Both hooks exchange information and data for the synchronization of the global execution through a *"first in first out"* (FIFO), also called a *"named pipe"*, with an ad-hoc protocol, see Fig. 16. This is an efficient and portable way of communication between processes and is part of the standard C library (*"libc"*). There is a restriction related to this implementation: inter-process communication via FIFO can only be done between processes in the same host, constraining the master processes of both PETSc-FEM modules to be executed at the same computing node. That is, the parallel runs (fluid and mesh-movement) can be executed on the same set of nodes (see Fig. 17), or in different ones. However, their master processes (MPI rank 0) must be the same (see Fig. 18). This restriction could be removed by replacing the FIFO by a socket.

The sequence of the process is the following. First, the Navier-Stokes solver calculates the state in the fluid. Then, the velocities on the surface nodes are sent to the pseudo-elastic solver which computes the new free surface node positions and solves the pseudo-elastic problem. The new fluid nodes coordinates are sent back to the fluid solver, which computes the fluid node mesh velocities, needed for computing the ALE terms. Then the fluid solver computes the fluid state and the whole process is restarted. In summary, the

communication between the modules at each time step amounts only to sending the free surface velocities to the pseudo-elastic solver, and the fluid nodes positions back. Note that, as the mesh partitioning for both modules is the same, much of this traffic is *inside* each processor, so that no communication overhead is caused.

Further developments and examples of free-surface flows with mesh movement solved by parallel computation were published by Tezduyar [17] *et al.* and Johnson [19] *et al.*

References

[1] Housner, G. W., 1957. "Dynamic pressures on accelerated fluid containers". *Bulletin of Seismic Society of America,* **47**, pp. 15–35.

[2] Storti, M. A., and D'Elía, J., 2005. "Added mass of an oscillating hemisphere at very-low and very-high frequencies". *ASME-J. of Fluids Engng.,* **126**(6), November, pp. 1048–1053.

[3] Biswal, K. C., Bhattacharyya, S. K., and Sinha, P. K., 2004. "Dynamic response analysis of a liquid-filled cylindrical tank with annular baffle". *Journal of Sound and Vibration,* **274**(1), pp. 13–37.

[4] Shyy, W., Udaykumar, H. S., Rao, M. M., and Smith, R. W., 1996. *Computational Fluid Dynamics with Moving Boundaries.* Taylor and Francis.

[5] Aliabadi, S., and Tezduyar, T. E., 2000. "Stabilized-finite-element/interface-capturing technique for parallel computation of unsteady flows with interfaces". *Computer Methods in Applied Mechanics and Engineering,* **190**, pp. 243–261.

[6] Perot, B., and Nallapati, R., 2003. "A moving unstructured staggered mesh method for the simulation of incompressible free-surface flows". *Journal of Computational Physics,* **184**(1), pp. 192–214.

[7] Nickell, R. E., Tanner, R. I., and Caswell, B., 1974. "The solution of viscous incompressible jet and free-surface flows using finite element method". *Journal of Fluid Mechanics,* **65**, pp. 189–206.

[8] Silliman, W. J., and Scriven, L. E., 1980. "Separating flow near a static contact line: slip at the wall and shape of a free surface". *Journal of Computational Physics,* **34**(3), pp. 287–313.

[9] Ruschak, K. J., 1980. "A method of incorporating free boundaries with surface tension in finite element fluid flow simulation". *International Journal for Numerical Methods in Engineering,* **15**(5), pp. 639–648.

[10] Kawahara, M., and Miwa, T., 1984. "Finite element analysis of wave motion". *International Journal for Numerical Methods in Engineering,* **20**(7), pp. 1193–1210.

[11] Bach, P., and Hassager, O., 1985. "An algorithm for the use of the lagrangian specification in newtonian fluid mechanics and applications to free-surface flows". *Journal of Fluid Mechanics,* **152**, pp. 173–190.

[12] Ramaswamy, B., and Kawahara, M., 1987. "Lagrangian finite element analysis applied to viscous free surface fluid flow". *International Journal for Numerical Methods in Fluids,* **7**(9), pp. 953–984.

[13] Hughes, T. J. R., Liu, W. K., and Zimmermann, T. K., 1981. "Lagrangian-Eulerian finite element formulation for incompressible viscous flows". *Computational Methods in Applied Mechanics and Engineering,* **29**, pp. 329–349.

[14] Sung, J., Choi, H. G., and Yoo, J. Y., 2000. "Time-accurate computation of unsteady free surface flows using an ALE-segregated equal-order FEM". *Comput. Methods Appl. Mech. Engrg.,* **190**, pp. 1425–1440.

[15] Huang, Y., and Sclavounos, P. D., 1998. "Nonlinear ship motions". *Journal of Ship Research,* **42**(2), pp. 120–130.

[16] York, A. R., Sulsky, D., and Schreyer, H. L., 2000. "Fluid-membrane interaction based on the material point method". *International Journal for Numerical Methods in Engineering,* **48**(6), pp. 901–924.

[17] Tezduyar, T., Aliabadi, S., Behr, M., Johnson, A., and Mittal, S., 1993. "Parallel finite-element computation of 3d flows". *Computer,* **26**, pp. 27–36.

[18] Tezduyar, T. E., Behr, M., Mittal, S., and Johnson, A. A., 1992. "Computation of unsteady incompressible flows with the stabilized finite element methods–space-time formulations, iterative strategies and massively parallel implementations". In *New Methods in Transient Analysis*, PVP-VOL.246/AMD-Vol.143. ASME, New York, pp. 7–24.

[19] Johnson, A. A., and Tezduyar, T. E., 1994. "Mesh update strategies in parallel finite element computations of flow problems with moving boundaries and interfaces". *Computer Methods in Applied Mechanics and Engineering,* **119**, pp. 73–94.

[20] D'Elía, J., Storti, M. A., Oñate, E., and Idelsohn, S. R., 2002. "A lagrangian panel method in the time domain for moving free-surface potential flows". *International Journal of Computational Fluid Dynamics,* **16**(4), pp. 263–275.

[21] D'Elía, J., Storti, M. A., and Idelsohn, S. R., 2001. "A surface remeshing for floating-like bodies with a moving free surface". In Mecánica Computacional, Vol. 20, XII Congress on Numerical Methods and their Applications - ENIEF 2001, pp. 462–467.

[22] Hughes, T. J. R., and Brooks, A. N., 1979. "A multidimensional upwind scheme with no crosswind diffusion". In *Finite Element Methods for Convection Dominated Flows*, ASME, ed., Vol. 34. AMD, New York, pp. 19–35.

[23] Brooks, A. N., and Hughes, T. J. R., 1982. "Streamline upwind/Petrov-Galerkin formulations for convection dominated flows with particular emphasis on the incompressible Navier-Stokes equations". *Computer Methods in Applied Mechanics Engineering,* **32**, pp. 199–259.

[24] Tezduyar, T. E., 1992. "Stabilized finite element formulations for incompressible flow computations". *Advances in Applied Mechanics,* **28**, pp. 1–44.

[25] Tezduyar, T. E., Mittal, S., Ray, S. E., and Shih, R., 1992. "Incompressible flow computations with stabilized bilinear and linear equal order interpolation velocity-pressure elements". *Computer Methods in Applied Mechanics and Engineering,* **95**, pp. 221–242.

[26] Behr, M., and Abraham, F., 2002. "Free-surface flow simulations in the presence of inclined walls". *Computational Methods in Applied Mechanics and Engineering,* **191**, p. 54675483.

[27] Güler, I., Behr, M., and Tezduyar, T., 1999. "Parallel finite element computation of free-surface flows". *Computational Mechanics,* **23**(2), pp. 117–123.

[28] PETSc-FEM: a general purpose, parallel, multi-physics FEM program. GNU General Public License (GPL), http://www.cimec.org.gov.ar/petscfem.

[29] Sonzogni, V. E., Yommi, A. M., Nigro, N. M., and A., S. M., 2002. "A parallel finite element program on a Beowulf Cluster". *Advances in Engineering Software,* **33**, pp. 427–443.

[30] Paz, R. R., and Storti, M. A., 2005. "An interface strip precondition for domain decomposition methods: application to hydrology". *International Journal for Numerical Methods in Fluids,* **62**(13), pp. 1873–1894.

[31] Paz, R. R., Nigro, N. M., and Storti, M. A., 2005 (in press). "On the efficiency and quality of numerical solutions in CFD problems using the interface strip preconditioner for domain decomposition methods". *International Journal for Numerical Methods in Fluids.*

[32] Braza, M., Chassaing, P., Chassaing, H., and Minh, H., 1986. "Numerical study and physical analysis of the pressure and velocity fields in the near wake of a circular cylinder". *Journal of Fluid Mechanics,* **165**, pp. 79–130.

[33] Tezduyar, T. E., and Shih, R., 1991. "Numerical experiments on downstream boundary of flow past cylinder". *Journal of Engineering Mechanics,* **117**, pp. 854–871.

[34] Behr, M., Liou, J., Shih, R., and Tezduyar, T. E., 1991. "Vorticity-stream function formulation of unsteady incompressible flow past a cylinder: sensitivity of the computed flow field to the location of the outflow boundary". *International Journal for Numerical Methods in Fluids,* **12**, pp. 323–342.

[35] Cantwell, B. J., and Coles, D., 1983. "An experimental study of entrainment and transport in the turbulent near wake of a circular cylinder". *Journal of Fluid Mechanics,* **136**, pp. 321–374.

[36] Roshko, A., 1961. "Experiments on the flow past a circular cylinder at very high Reynolds number". *Journal of Fluid Mechanics,* **10**, pp. 345–356.

[37] Williamson, C. H. K., 1996. "Vortex dynamics in the cylinder wake". *Annual Review of Fluid Mechanics,* **28**, pp. 477–539.

[38] Gushchin, V., Kostomarov, A., Matyushin, P., and Pavlyukova, E., 2002. "Direct numerical simulation of the transitional separated fluid flows around a sphere and a circular cylinder". *Journal of Wind Engineering,* **90**, pp. 341–358.

[39] Mittal, R., and Balachandar, S., 1995. "Effect of three-dimensionality on the lift and drag of nominally two-dimensional cylinders". *Physics of Fluids,* **7**(8), pp. 1841–1865.

[40] Norberg, C., 2001. "Flow around a circular cylinder: aspects of fluctuating lift". *Journal of Fluids and Structures,* **15**, pp. 459–469.

[41] Rabier, S., and Medale, M., 2003. "Computation of free surface flows with a projection FEM in a moving mesh framework". *Computer Methods in Applied Mechanics,* **192**, pp. 4703–4721.

[42] Prosperetti, A., 1981. "Motion of two superposed viscous fluids". *Physic of Fluids,* **24**(7), July, pp. 1217–1223.

[43] Papaspyrou, S., Karamanos, S. A., and Valougeorgis, D., 2004. "Response of half full horizontal cylinders under transverse excitation". *Journal of Fluids and Structures,* **19**(7), pp. 985–1003.

[44] Moiseev, N. N., and Petrov, A. A., 1966. "The calculation of free oscillations of a liquid in a motionless container". In *Advances in Applied Mechanics*, Vol. 9. Academic Press, pp. 91–155.

[45] Message passing interface (MPI). http://www.mpi-forum.org/docs/docs.html.

[46] Balay, S., Gropp, W., McInnes, L. C., and Smith, B., 1997. Petsc 2.0 users manual. Tech. Rep. UC-405, Argonne National Laboratory.

[47] D'Elía, J., Storti, M., and Idelsohn, S., 2000. "A panel-Fourier method for free surface flows". *ASME-J. of Fluids Engng.,* **122**(2), June, pp. 309–317.

[48] Linux. The Linux Documentation Project, http://www.gnu.org.

List of Figures

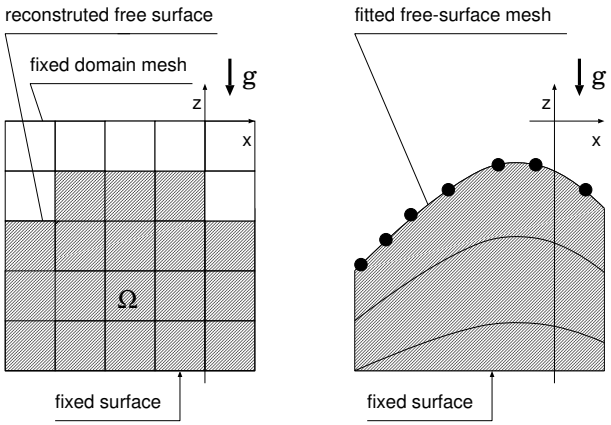

Figure 1: A flow domain with a free surface discretized by domain-like schemes: Eulerian-type (left) and Lagrangian-type (right) methods.

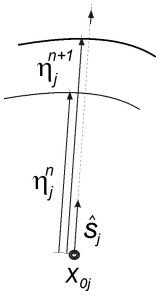

Figure 2: Notation for the spines-like employed in the mesh-movement.

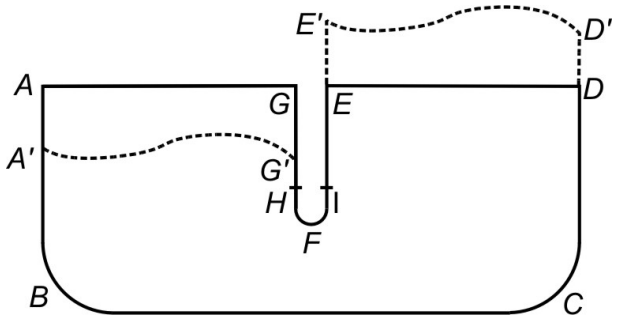

Figure 3: Boundary conditions for the pseudo elastic problem for a mesh movement: nodes can move freely at the solid walls $ABCD$, GH and IE (slip boundary condition) and non-slip one in portion HFI to prevent large distortions of elements near the tip F of the separator.

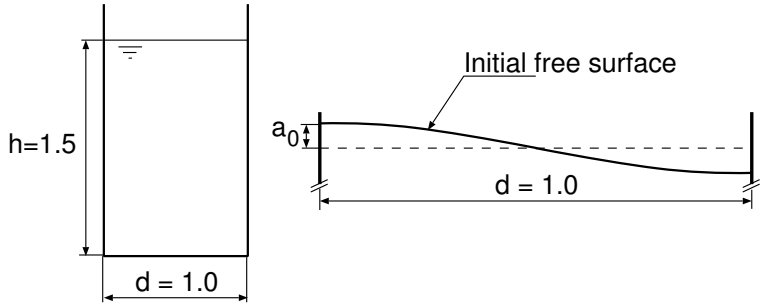

Figure 4: Dimensions in m and initial free surface position for the sloshing problem with known solution.

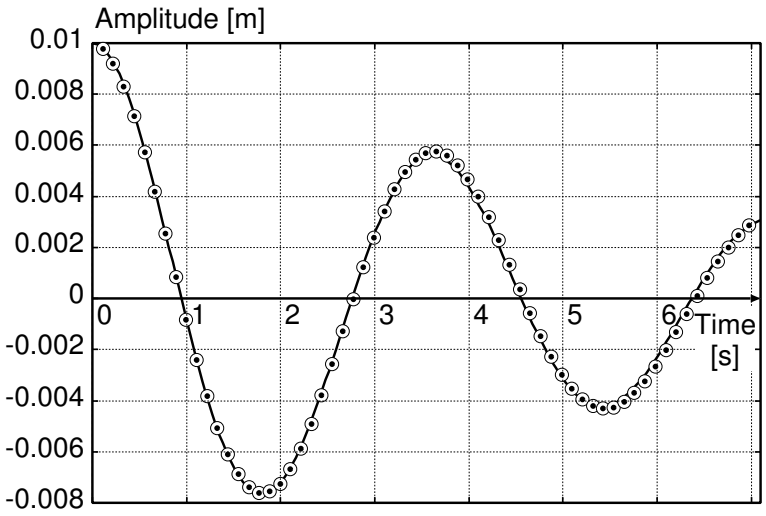

Figure 5: Analytic solution curve and numerical results (dots) calculated for the sloshing problem.

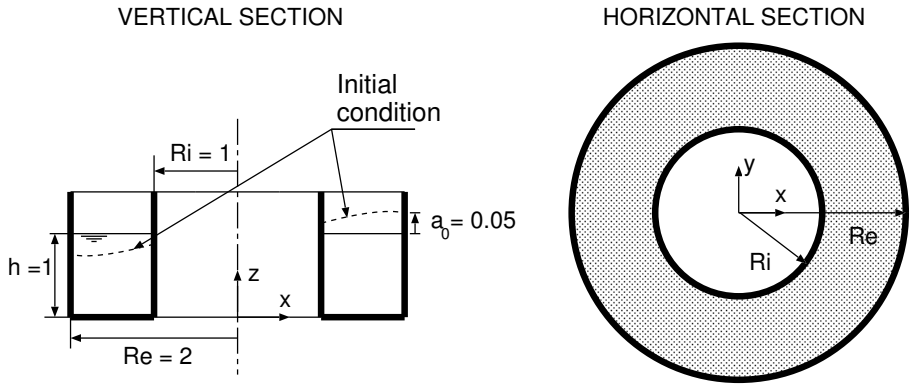

Figure 6: Vertical and horizontal sections of a right vertical cylinder with annular base for a three-dimensional quasi-inviscid sloshing test. Initial free surface and reference axis. Dimensions in m.

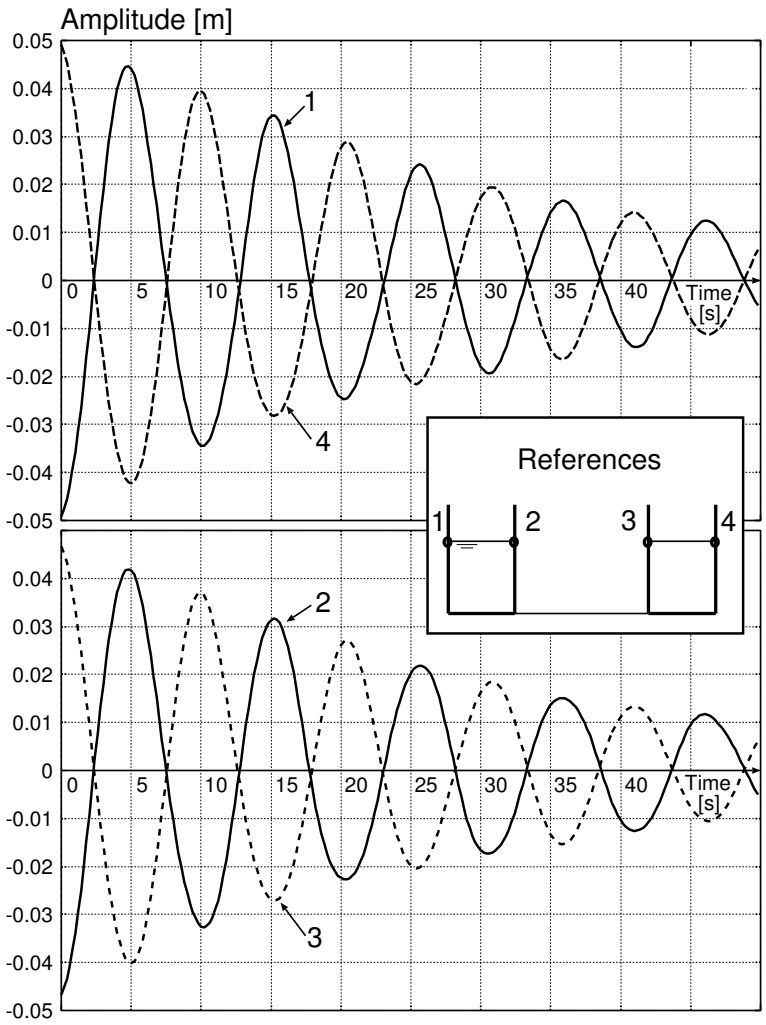

Figure 7: Displacements time evolution for some representative mesh-nodes in the tank of annular base.

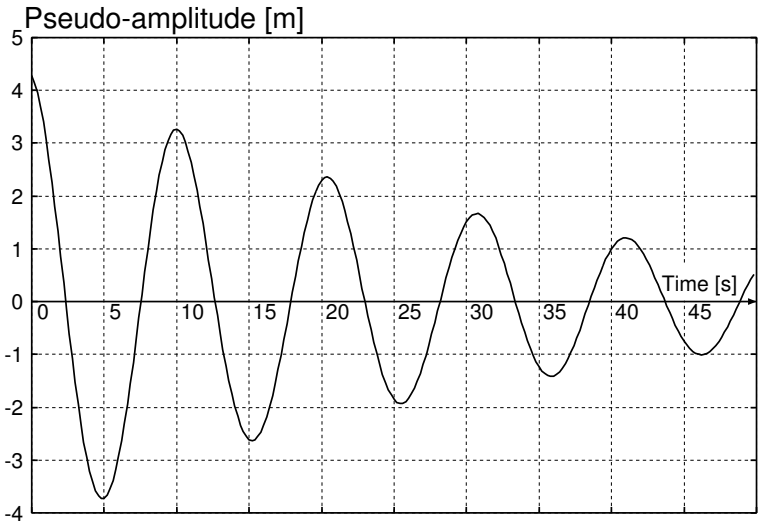

Figure 8: Filtered nodes movement on the free surface for the 3D cylindrical tank.

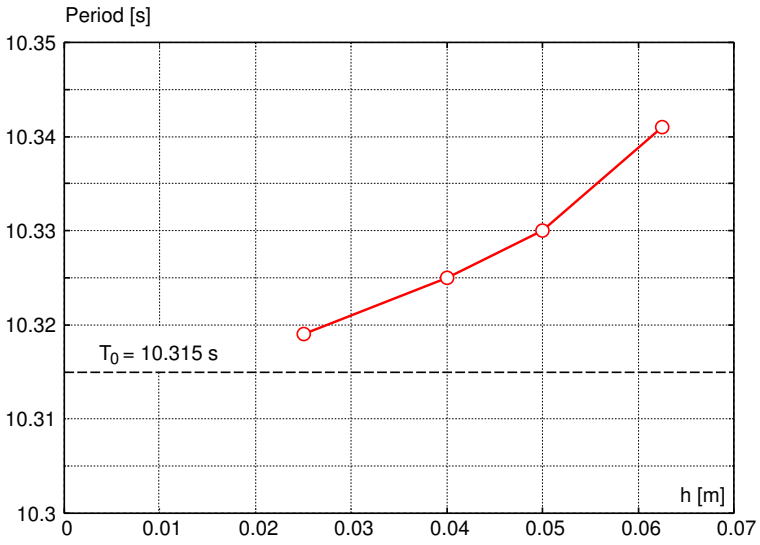

Figure 9: Period of movement T versus mesh mean step h for the sloshing 3D test.

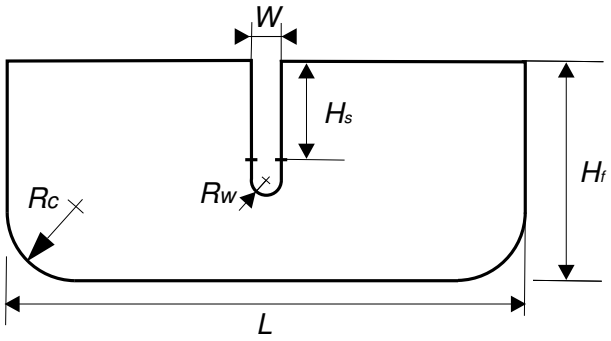

Figure 10: Main geometrical dimensions of a truck-like container with a separating wall.

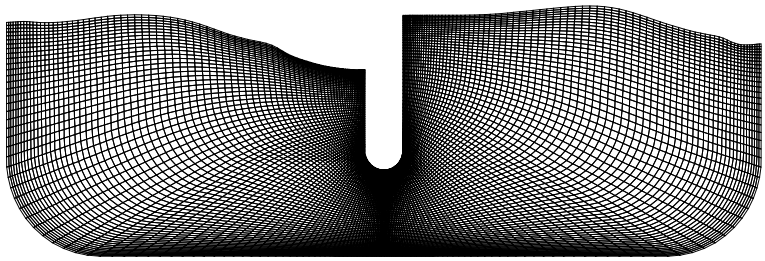

Figure 11: Updated mesh with a pseudo elastic strategy.

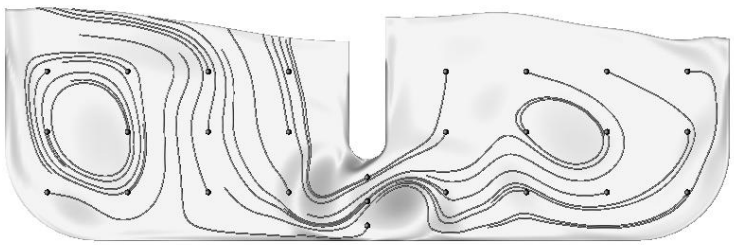

Figure 12: Vorticity and streamlines at time step $n_t = 209$. A forming vortex is clearly formed on the left wall of the separator near the tip.

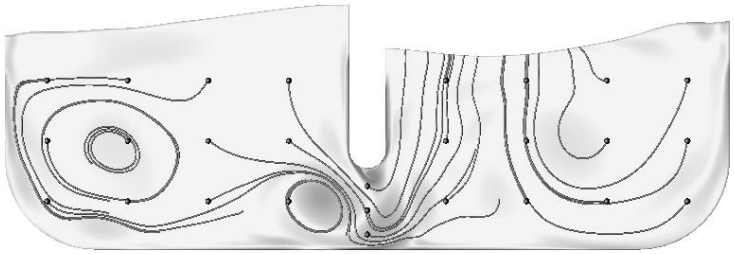

Figure 13: Vorticity and streamlines at time step $n_t = 217$. The previously formed vortex has been separated from the wall.

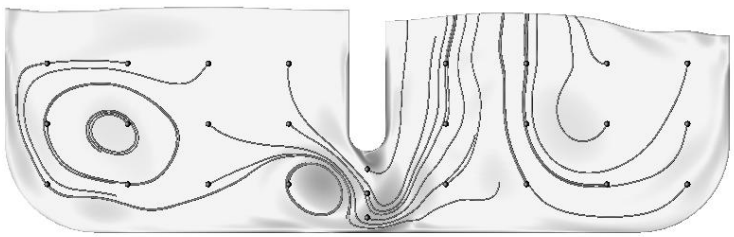

Figure 14: Vorticity and streamlines at time step $n_t = 224$. Once the vortices are shed they are transported by the fluid.

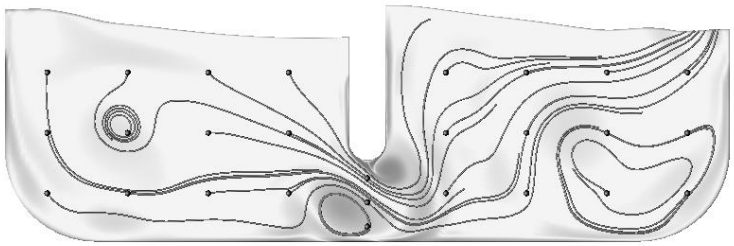

Figure 15: Vorticity and streamlines at time step $n_t = 230$. A new vortex forming on the right half.

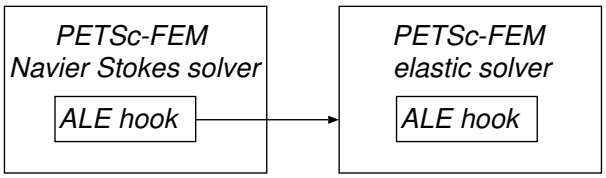

Figure 16: PETSc-FEM hooks that exchange information and data for the synchronization of the global execution of the fluid and pseudo elastic solvers.

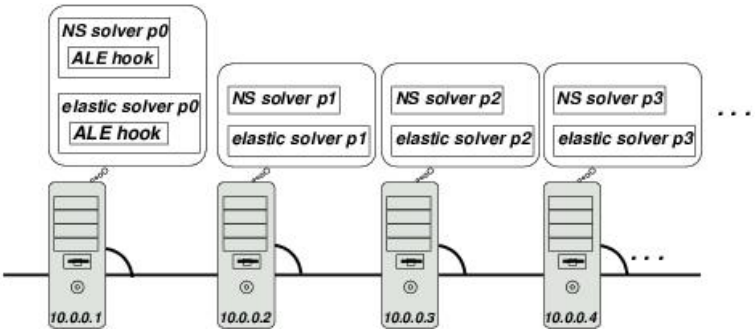

Figure 17: The master processes of both PETSc-FEM (fluid and mesh-movement) are executed at the same computing node.

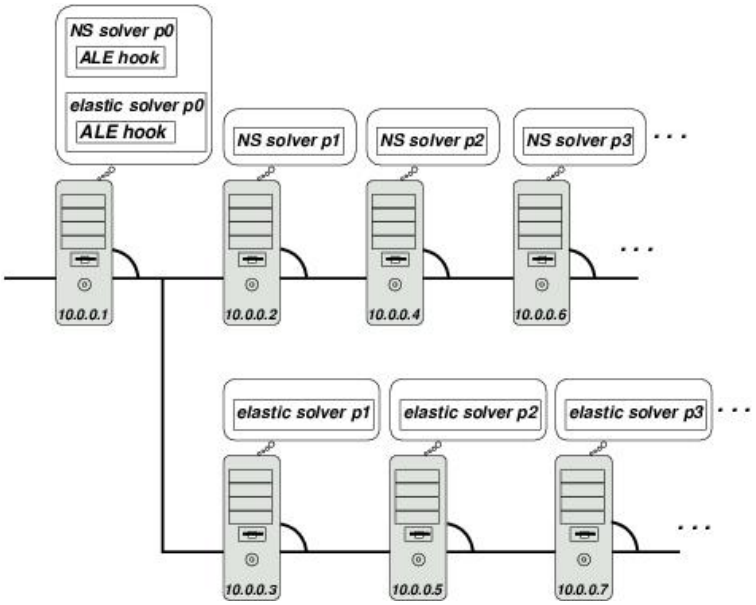

Figure 18: The PETSc FEM parallel runs (fluid and mesh-movement) are running in different node sets but their master processes (MPI rank 0) must be the same.